Received: 28 September 2021 | Revised: 7 November 2021 | Accepted: 21 November 2021

DOI: 10.1002/fsn3.2696

Food Science & Nutrition Open Access WILEY

ORIGINAL RESEARCH

Ultrasound-assisted solubilization of calcium from micrometer-scale ground fish bone particles

Juanjuan Guo[1,2,3] | Siliang Zhu[1,2] | Hongbin Chen[1,3] | Zongping Zheng[1,3] | Jie Pang[2]

[1]College of Oceanology and Food Sciences, Quanzhou Normal University, Quanzhou, China

[2]College of Food Science, Fujian Agriculture and Forestry University, Fuzhou, China

[3]Key Laboratory of Inshore Resources Biotechnology (Quanzhou Normal University) Fujian Province University, Quanzhou, China

Correspondence
Juanjuan Guo, College of Oceanology and Food Sciences, Quanzhou Normal University, Quanzhou, Fujian 362000, China.
Email: gjjfst15@163.com

Funding information
The Talent Introduction and Research Launch Project of Quanzhou Normal University, Grant/Award Number: H19007; the High-Value Development and Utilization of Marine Fish Processing By-Products, Grant/Award Number: 2018CT004; National Natural Science Foundation of China, Grant/Award Number: 32001625

Abstract

In order to promote the extraction of biological calcium from fish bone, ultrasonication was used to process micrometer-scale fish bone particles (MFPs) and investigate the mechanism of action in relation to bone structure. With ultrasonication treatment (300 W, 60°C, 2 h), the content of calcium release increased by 25.6%. Calcium release reached 94.0% of total calcium after 24-h treatment. The surface of the MFPs was significantly damaged by ultrasound-induced cavitation, resulting in holes and separation of the layered structure. X-ray diffraction (XRD) and Fourier transform infrared (FT-IR) analysis demonstrated that the crystalline structure of hydroxyapatite was disrupted, the triple helical structure of mineralized collagen fibrils (MCFs) was loosened, and hydrogen bonding in collagen decreased, facilitating the release of hydroxyapatite crystals. Thus, ultrasonication may be a practical alternative to nanomilling for industrial processing of waste fish bones to produce soluble calcium as an ingredient in calcium supplements and supplemented foods.

KEYWORDS
calcium release, fish bone particles, mineralized collagen fibrils, ultrasonication

1 | INTRODUCTION

Leftovers (e.g., fish bone, skin, and fish viscera) from fish processing are causing increasing environmental problems with the rapid growth of the global fishing industry (Marliana et al., 2015). These leftovers, however, are rich in nutrients, such as proteins, lipids, and minerals. Fish bones are a major by-product of fish processing and are a potential biological source of natural inorganic calcium (Xu et al., 2020). Some research has been undertaken on the utilization of calcium from fish bones, for example, using it to make calcium-fortified food. However, conversion of fish bones into a bioavailable form of calcium that is easily absorbed from the digestive system is difficult, and there is a clear need for effective processing methods to achieve this industrially (Li et al., 2020; Yin et al., 2015).

Mackerel (*Trachurus trachurus*), a low-value bulk fish, has been used as a source of fish bones for processing to extract calcium (Ferraro et al., 2013). Calcium in Mackerel bones is in the form of hydroxyapatite (HA) and β-tricalcium phosphate (Terzioglu et al., 2018). The main components of fish bones are the inorganic phase (calcium phosphate, CaP) ceramics (mainly hydroxyapatite (HA) crystals) and the organic/protein phase (mineralized collagen fibrils, MCFs), which form a complex matrix (Xu et al., 2020). The MCFs (mainly collagen-I, 90%) have a triple helical collagen structure and act as an adhesive, strongly binding to hydroxyapatite, and giving the bone stiffness and

resilience. Since hydroxyapatite crystals are embedded in the collagen matrix, it is extremely difficult to extract calcium from them. The common current method to promote calcium release from fish bones is grinding the material into nanometer-scale particles. For example, high-energy wet ball milling can grind fish bones into particles with an average size of 110 nm, which increased the degree of calcium dissolution from 0.7% to 27.4% (Yin et al., 2016). Nanogrinding degrades the collagen-fiber network structure and breaks down the hydroxyapatite crystals by collision and crushing (Eskin et al., 2005). Thermal treatment is another method to promote calcium release from fish bone through degradation of the collagen fiber matrix and reducing the mechanical strength of the bone. Heating effectively promoted calcium release from previously ground nanoscale fish bone particles (Jiang et al., 2020; Zhang et al., 2016). Therefore, degradation of the collagen matrix is an effective method to release calcium from fish bones. However, nanomilling is costly, and a feasible alternative technology to increase calcium release from microscale fish bone particles is indispensable.

Ultrasound waves in a liquid system generate cavitation bubbles, which grow larger by absorbing gas or vapor, then collapse, releasing the absorbed energy as heat and breaking up any solid material present, which has been reported that can disrupt the triple helical structure of collagen and facilitate the decalcification of bones in the medical field (Amiri et al., 2018). Ultrasonication has been used to extract gelatin from animal skins, by destabilizing the collagen structure and loosening the triple helical structure (Ali et al., 2018b). Ultrasound treatment has been used to extract collagen-II from chicken sternal cartilage; the triple helical structure was partially denatured after longer treatment times (Akram & Zhang, 2020). Ultrasound treatment has also been used for decalcification of bones, or organs in the medical field, indicating that it should be able to release calcium from fish bones (Chen et al., 2007; Milan & Trachtenberg, 1981). However, to our knowledge, there has been no report on the extraction of soluble calcium from fish bones using ultrasonication.

In this study, fish bone particles in the micrometer size range were made from Mackerel bones by ultrafine friction milling. Changes in the physicochemical properties (particularly calcium release and micromorphology) of fish bone particles during ultrasound treatment were investigated and compared. The mechanism by which ultrasound treatment promotes calcium release from fish bone particles was analyzed to help provide a theoretical basis for the practical industrial extraction of soluble biological calcium from fish bones.

2 | MATERIALS AND METHODS

2.1 | Materials

Mackerel (36 cm length, 457 g/fish) were provided by Ruifang Food Co., Ltd., Quanzhou, China. Mackerel were filleted and deboned using a roll-type meat separator (YBYM-6004-B, Yingbo Food Machinery Co., Ltd.), and fish backbones were collected. The fish backbones were cleaned two to three times using deionized water to remove blood and flesh, and then stored at −20°C. All reagents used were of analytical grade from local suppliers.

2.2 | Preparation of coarse fishbone particles (CFPs) and micrometer fishbone particles (MFPs)

Frozen fish backbones were thawed at room temperature, cut with a knife into pieces 5–10 cm long, then immersed in 40% aqueous Na_2CO_3 at a ratio of 1:3 (w/v), and autoclaved at 121°C (100 kPa) for 1 h to remove connective tissue and fat. The cooled, separated vertebrae were cleaned two to three times using deionized water and dried at 105°C for 1 h.

Coarse fishbone particles (CFPs): The fish vertebrae were ground using a high-speed pulverizer (FW100, 50 Hz, Tester Instruments Co. Ltd) at a speed of 4,500 rpm for 60 s.

Micrometer fishbone particles (MFPs): The CFPs were further ground using an ultrafine friction grinder (PX-MFC 90D, WIGGENS) at a speed of 3,000 rpm for 45 s.

2.3 | Determination of particle size

The mean particle size and particle size distribution of CFPs and MFPs were determined by laser light-scattering, using a Microtrac S3500 analyzer (Microtrac Inc.). The particle sizes of CFPs and MFPs in the micrometer range (1–1,000 μm) were measured, and the results were analyzed with Microtrac S3500 software using a Mie scattering model. Raw data were drawn with Origin 8.5 software.

2.4 | Determination of content of calcium release

The content of calcium release was determined under an in vitro-simulated digestion system to digest samples according to a previously described method (Zhang et al., 2017). Samples (3 g) were dissolved in simulated gastric fluid (SGF, 100 ml). SGF was composed of KCl (6.9 mM), NaCl (42.7 mM), $CaCl_2.2H_2O$ (0.15 mM), $NaHCO_3$ (25 mM), KH_2PO_3 (0.9 mM), $MgCl_2(H_2O)_6$ (0.12 mM), $(NH_4)_2CO_3$ (0.5 mM), and HCl (15.6 mM) (Brodkorb et al., 2019). The pH was adjusted to 3.0 ± 0.2 using 6 mol/L HCl and porcine pepsin solution (0.5 ml, 3200 U/mg, Sigma-Aldrich) was added to achieve an activity of 2,000 U/mL in the final digestion mixture. The mixture was incubated in a constant temperature shaker at 37°C and 140 rpm/min for 2 h, and then, the samples were centrifuged at 3996 *g* for 20 min and the supernatant was filtered and diluted with deionized water. Additionally, the factors in simulated gastric fluid including enzyme (porcine pepsin, other enzymes), pH (pH = 1, 3, 5 and 7) and digested time (0, 1, 2, 4, 6, and 8 h), were further investigated to explore the optimal factors. The kinetics of ultrasonic treatment time was also conducted. The calcium concentration was measured using an atomic absorption spectroscope (A3,

Beijing Purkinje General Instrument Co. Ltd) as the method of GB/T 5009.92-2003; the determination parameters were set to wavelength of 422.7/nm, height of burning head 6/mm, lamp current of 3/mA, flame Air-Acetylene, acetylene flow rate of 1500 L/min.

2.5 | Determination of chemical components

The contents of moisture, ash, fat, protein, phosphorus, and heavy-metal ions including, Pb, As, Hg, Cd, and Cr, were detected according to Jin Zhang and Pham Viet Nam's methods (Nam et al., 2019; Zhang et al., 2016, 2017). The inductively coupled plasma-optical emission spectrometry (ICP-OES) analysis was performed using a PerkinElmer Optima 4300 DV spectrometer.

2.6 | Ultrasound-assisted calcium extraction

Control group: MFPs (3 g) were added to 100 ml simulated gastric fluid as described above without adding a digestive enzyme, and the mixture was incubated as described in Section 2.4. Ultrasound-treated fish bone particles (U-MFPs): MFPs (3 g) were added to 100 ml simulated gastric fluid as described above without adding a digestive enzyme, and the mixture was prepared using an ultrasonic extractor SCIENTZ-IIDM (Ningbo Scientz Biotechnology Co., LTD) equipped with an amplitude transformer-Φ6. To optimize the ultrasound treatment conditions, ultrasound treatment was performed at a fixed frequency (20 kHz), but the power (100, 300, and 500 W) at temperature 37°C for 2 h, temperature (37, 60, and 85°C) at power 300 W for 2 h and time (0, 1, 2, 3, 4, 6, 8, 10, 12, 14 and 24 h) at 300 W, 60°C were varied. The processing mode was tip-type, and the extractor was operated in a pulsed mode, with 5-s sonication and 5-s resting time, in order to avoid over-heating of the reaction system.

2.7 | Mathematical fitting of calcium release with ultrasonic treatment

The Higuchi equation (Equation 1) and zero-order kinetic function (Equation 2) were used to curve-fit calcium release after ultrasonic treatment. The mathematic models were as follows:

$$R(t) = R_0 + kt^{1/2} \quad (1)$$

$$R(t) = R_0 + kt \quad (2)$$

where R_0 is the initial calcium release of MFPs (mg/g_{MFPs}), k is a calcium release constant, which can be determined by linear regression analysis between $R(t)$ and ultrasonication time$^{1/2}$, t is the ultrasonication time (h), and $R(t)$ is the calcium release after a given ultrasonication time (mg/$g_{U\text{-}MFPs}$). A higher k value corresponds to a higher overall release rate.

2.8 | Characterization of CFPs, MFPs, and U-MFPs

2.8.1 | Morphological observation

The microstructures of CFPs, MFPs and ultrasound treated samples (U-MFPs) were visualized using a scanning electron microscope (SEM; JSM-6380LV, Tokyo, Japan). Before scanning, samples were mounted on a bronze stub and sputter-coated with gold. The instrument settings were as follows: accelerating voltage, 5.0 kV, and magnification, ×50,000.

2.8.2 | Fourier-transform infrared spectroscopy (FTIR)

FTIR was used to analyze the functional groups present in inorganic hydroxyapatite and organic mineralized collagen fibrils (MCFs). The samples were vacuum freeze-dried and recorded using a Nicolet™ 360 FTIR spectrometer (Thermo Fisher Scientific, Waltham, MA). A spectral range from 500 to 4000 cm^{-1} with a resolution of 2 cm^{-1} was analyzed.

2.8.3 | X-ray diffraction (XRD)

The samples were vacuum freeze-dried, and crystal structural analysis of hydroxyapatite and MCFs was performed using an X-ray diffractometer (Rigaku TTR-III, Rigaku) with a Cu$K\alpha$ X-ray source ($\lambda = 1.54178$, generator voltage of 40 kV, incident current of 200 mA). Scanning was carried out from 5 to 50° at a scan rate of 0.02 deg/s.

2.9 | Statistical analysis

All experiments were performed in triplicate with a completely randomized design. Analysis of variance (ANOVA) and regression was accomplished using Statistical Analysis System software (SAS Institute). Differences between mean values were determined by Duncan's multiple range tests.

3 | RESULTS AND DISCUSSION

3.1 | Particle size and morphology of CFPs and MFPs

The mean diameter of the volume distribution (MV) was 124.6 μm for CFPs, markedly higher than that of MFPs (MV = 68.5 μm) (Figure 1a). The distribution peak at D_{50} = 337.9 μm for CFPs was absent after ultrafine friction treatment and the size distribution of MFPs contained few particles larger than 300 μm. The volume % of particles larger than 200 μm reduced from 27.5% in CFP material

to 2.8% in MFP. The ultrafine friction treatment effectively reduced the particle size of ground fish bones. The reduced particle size after ultrafine friction treatment was also apparent from SEM imaging (Figure 1b). However, the surface morphology of CFPs and MFPs did not appear significantly different, suggesting that ultrafine friction treatment did not disrupt the internal structure of the particles, which is necessary to efficiently release soluble calcium. Compositional analysis of CFPs and MFPs (Table 1) revealed some significant differences. The contents of fat, protein, and phosphorus decreased after ultrafine friction treatment. The contents of moisture (2.7%–3.0%) and calcium (152–175 mg/g) increased in MFPs. What is more, the contents of heavy metal ions were significantly decreased after ultrafine friction treatment, and within the range of Chinese standards. A previous report demonstrated that reduction in fish bone particle size facilitates calcium release, because of larger specific surface area and increased porosity, which facilitates the access of acid to the inorganic phase of the particles (Jeong et al., 2013). For example, nanomilling increases calcium release from fish bone particles compared with micromilling (Li et al., 2020; Yin et al., 2015). In addition, thermal treatment of nanoscale fish bone particles was more effective in promoting calcium release than that on microscale particles (Zhang et al., 2016). However, nanomilling is costly and a feasible alternative technology to increase calcium release from microscale fish bone particles is indispensable.

3.2 | Calcium release

3.2.1 | Effect of digest factors

The assessment of calcium release was conducted in a simulated gastric system (Li et al., 2020; Yin et al., 2015); thus, the factors that might affect the calcium release in the simulated gastric system were explored. The pH (pH = 3) and digestive enzyme (pepsin) were the main factors in the gastric system that affected calcium release, so the effects of different enzymes and pH were investigated. Pepsin and other enzymes (trypsin, neutral protease, and papain) were applied to digest MFPs. However, enzymes other than pepsin, operating at their pH optima, had no effect on calcium release

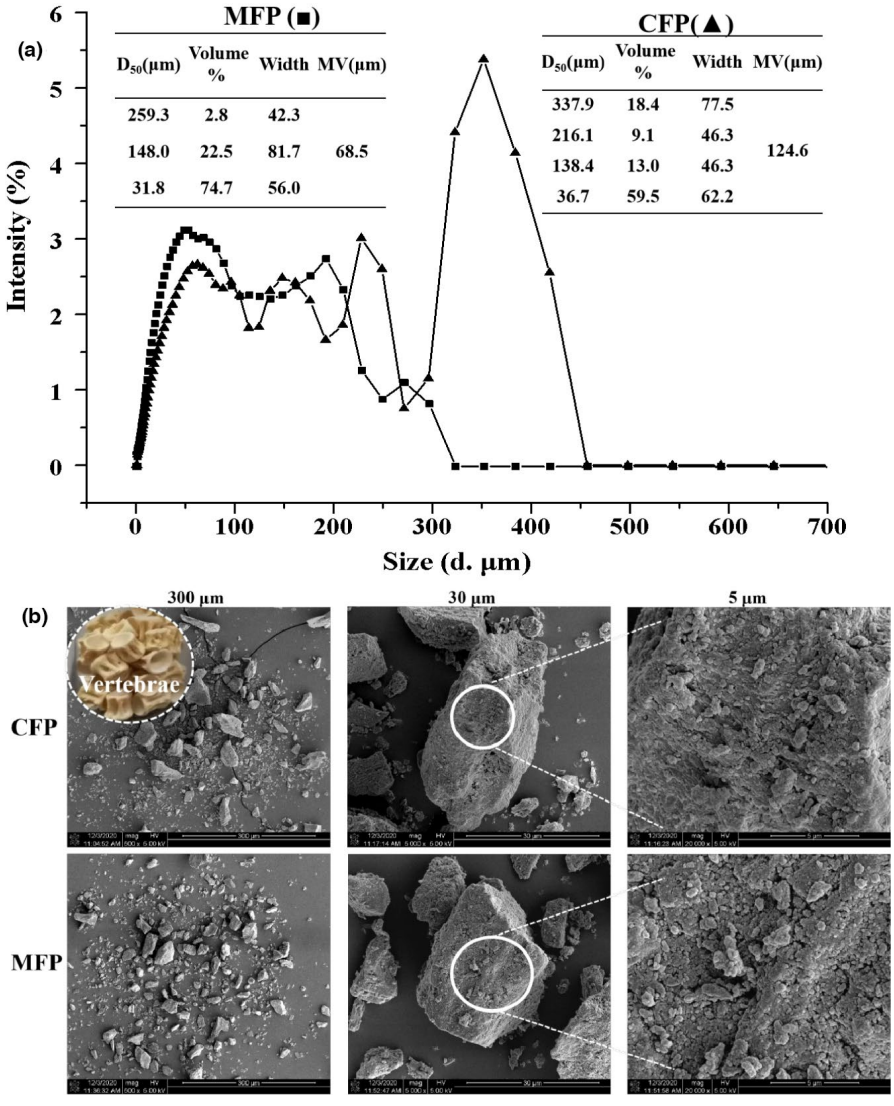

FIGURE 1 Particle size of CFPs and MFPs. (a) Particle size distribution and mean particle size (μm) of CFPs and MFPs. (b) Scanning electron microscopy images for CFPs and MFPs

TABLE 1 Component analysis of fish bone, CFPs, and MFPs

	Moisture (%)	Ash content (%)	Fat content (g/100 g)	Protein (g/100 g)	Calcium (mg/g)	Phosphorus (mg/g)	Ca:P
Fish bone	2.406 ± 0.262^{b}	79.631 ± 0.237^{a}	5.561 ± 0.132^{ab}	1.202 ± 0.080^{ab}	137.808 ± 2.429^{c}	116.907 ± 8.375^{b}	$1.179:1^{b}$
CFP	2.662 ± 0.011^{b}	79.239 ± 0.356^{a}	5.684 ± 0.338^{a}	1.211 ± 0.081^{a}	152.072 ± 2.655^{b}	127.858 ± 5.940^{a}	$1.189:1^{b}$
MFP	3.039 ± 0.095^{a}	78.528 ± 0.139^{ab}	5.470 ± 0.007^{b}	1.122 ± 0.001^{b}	174.894 ± 0.460^{a}	114.386 ± 8.308^{b}	$1.530:1^{a}$

	Pb (mg/kg)	As (mg/kg)	Hg (mg/kg)	Cd (mg/kg)	Cr (mg/kg)
Fish bone	0.701 ± 0.050^{a}	0.79 ± 0.010^{a}	–	0.017 ± 0.003^{b}	0.1 ± 0.030^{b}
CFP	0.239 ± 0.050^{b}	0.61 ± 0.010^{ab}	–	0.030 ± 0.003^{a}	0.34 ± 0.030^{a}
MFP	0.146 ± 0.050^{c}	0.48 ± 0.010^{b}	–	0.029 ± 0.003^{a}	0.22 ± 0.030^{ab}
Chinese standard	≤1.0	≤0.5	≤1.0	≤0.1	≤2.0

Note: Results are presented as mean ± *SD* ($n = 3$). Different lowercase letters within the same column indicate significant differences among fish bone, CFP, and MFP ($p < .05$).

Chinese standard: GB 2762-2017

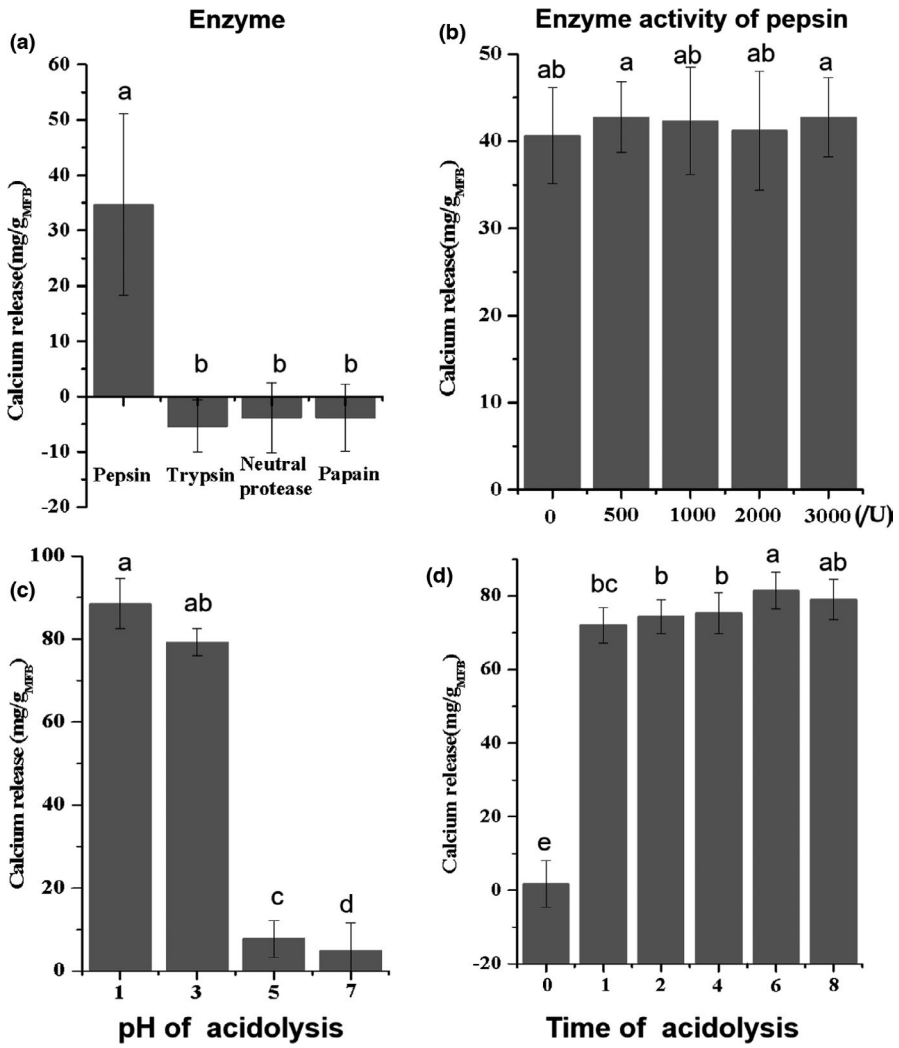

FIGURE 2 Effects of acid hydrolysis on the calcium release mean size of MFPs. a, b, c, and d represent enzyme, enzyme activity, pH, and acidolysis time, respectively

(Figure 2a). Moreover, the amount of calcium release was not significantly different with additions of pepsin between 0 and 3,000 U/mg, indicating that calcium release in the gastric system depends on acid hydrolysis, rather than on pepsin (Figure 2b). Varying the pH (Figure 2c) indicated that little calcium was released at pH above 3, but that pH 1 was only slightly more effective. The amount of calcium release did not change much after acid hydrolysis between 1 and 8 h (Figure 2d). Therefore, subsequent calcium release measurements were conducted in the simulated gastric system at pH 3, without pepsin present.

3.2.2 | Effect of ultrasound

Since ultrasonication can disrupt the triple helical structure of collagen and facilitate the decalcification of bones, the parameters of ultrasonic power, temperature, and treatment time were systematically varied to optimize ultrasound-assisted acid hydrolysis and promote calcium release from MFPs. The amount of calcium released increased with ultrasonic power, and at 300 W, was about 1.3 times that of the no-ultrasonication control ($p < .05$, Figure 3a). Ultrasonic treatment temperature also influenced calcium release, reaching a maximum of 107.5 mg/g MFPs (64%) at 60°C (Figure 3b). However, this figure was only slightly higher than that achieved at the 300 W power setting, indicating that temperature has minimal influence on ultrasonication-assisted calcium release. This is in contrast with a report that thermal treatments increase calcium release from fish bone particles during high-energy wet ball milling (Zhang et al., 2016). This appears to be because the particles in this study were of micrometer scale, rather than nanometer scale (Jiang et al., 2020). Calcium release significantly, but very gradually, increased with increasing treatment time (Figure 3b), reaching 94.0% after 24 h at 300 W and 60°C, compared with 53.0% after 0.5 h.

3.2.3 | Kinetics of ultrasonic treatment

The relationship between calcium release and ultrasonication time was fitted to the Higuchi function (Section 2.2.5, Equation 1) and the zero-order kinetic function (Equation 2) (Table 2). The Higuchi function had a better correlation ($R^2 > 0.99$), similar to that in a previous report on the effect of thermal treatments on calcium release from fish bones during high-energy wet ball milling (Zhang et al., 2017). These data suggest that the effects of ultrasonic treatment on calcium release may be similar to that of high-energy wet ball milling.

3.3 | Characteristic of ultra-sonication of MPFs

3.3.1 | Surface morphology

The surface morphology of MFPs after different ultrasonic power, temperature, and time treatments is shown in Figure 4. The fish bones used were vertebrae (inset in Figure 4a1). Without ultrasonication, the surface of the MFPs was dense and ordered, with stacked layers of planar mineralized collagen fibrils (MCFs) and much smaller hydroxyapatite crystals. The MCFs were well ordered along the longitudinal axis, and hydroxyapatite crystals filled the intervals between adjacent MCFs in a staggered arrangement (Figure 4a1). After different ultrasonic power treatments, multilevel hierarchical structures were clearly visible. The MCFs appeared to be arranged in parallel, forming flat sheets, which had been partially separated by the ultrasonic treatment. It also appeared that many of the hydroxyapatite crystals had been removed, making the layered structure more clearly visible (Figure 4a2, a3, a4 in 300 μm and 30 μm magnification). It appears that disruption of the layered structure facilitates the release of hydroxyapatite crystals. Moreover, the MCFs displayed holes and damage to their edges, which became more prominent with increased ultrasonic power (Figure 4a2, a3, a4 in 5 μm magnification). Ultrasound waves cause the creation, growth, and collapse of bubbles in liquid, known as cavitation (Liew et al., 2015). The diffusion of solvent vapor into the bubbles leads to their growth and implosive collapse, producing a localized hotspot by adiabatic compression (Bastami & Entezari, 2012). The hot spots momentarily reach very high temperatures (5000–25,000 K) and can break intramolecular chemical bonds, especially in organic compounds (Neppolian et al., 2008). Therefore, it appears that cavitation disrupts the surface of MFPs, especially the organic collagen, to facilitate the release of hydroxyapatite crystals.

After ultrasonic treatment at different temperatures, the changes in morphology were similar (Figure 4b) to those in Figure 4a, but more pronounced. With treatment at 60°C, the damage was more severe and the holes were bigger (Figure 4b2). However, after treatment at 85°C, the particles appeared much more extensively disrupted, with the layered structure mostly separated and the layers broken into much smaller pieces, although calcium release did not increase further (Figure 4b3, Figure 3b). Increasing treatment time (at 300 W and 60°C) resulted in similar changes to those in Figure 4a, which became gradually more pronounced (Figure 4c). Therefore, ultrasonic cavitation could disrupt the layered structure of the MFPs resulting in the appearance of holes in the layers and the near disappearance of hydroxyapatite crystals from the outside of the particles and from between the separated layers.

3.3.2 | FT-IR spectra

Ultrasound waves can break down collagen by loosening or denaturing its triple helical structure (Ali et al., 2018a, 2018b). Ultrasound-assisted extraction of hydroxyapatite from Nile tilapia fish scales disrupted the collagen structure (Sricharoen et al., 2020). Ultrasonic-assisted extraction of nanocalcium from eggshell, which contains collagen, has also been reported (Liew et al., 2015), but the mechanism of promoting calcium release was not discussed. Therefore, this was explored in the study. The FTIR spectra of MFPs samples after ultrasonication (Figure 5) showed the characteristic bands of collagen in the untreated control samples, including peaks at 3,400.98 cm^{-1} (N-H stretching vibration of amide A band), and 2,923.53 and 2,855.86 cm^{-1} (C-H asymmetrical stretching and symmetrical vibration of amide B band). After ultrasonication treatment, the amide A band shifted and split into two bands at 3,471.56 and 3,559.80 cm^{-1}, corresponding to the O-H stretching mode of hydroxyapatite (Yin et al., 2016), except that the amide A band completely disappeared in the 85°C treatment samples. The intensity of the amide B bands (2,923.53 and 2,855.86 cm^{-1}) decreased to varying degrees in the U-MFP samples. Untreated MFPs showed clear

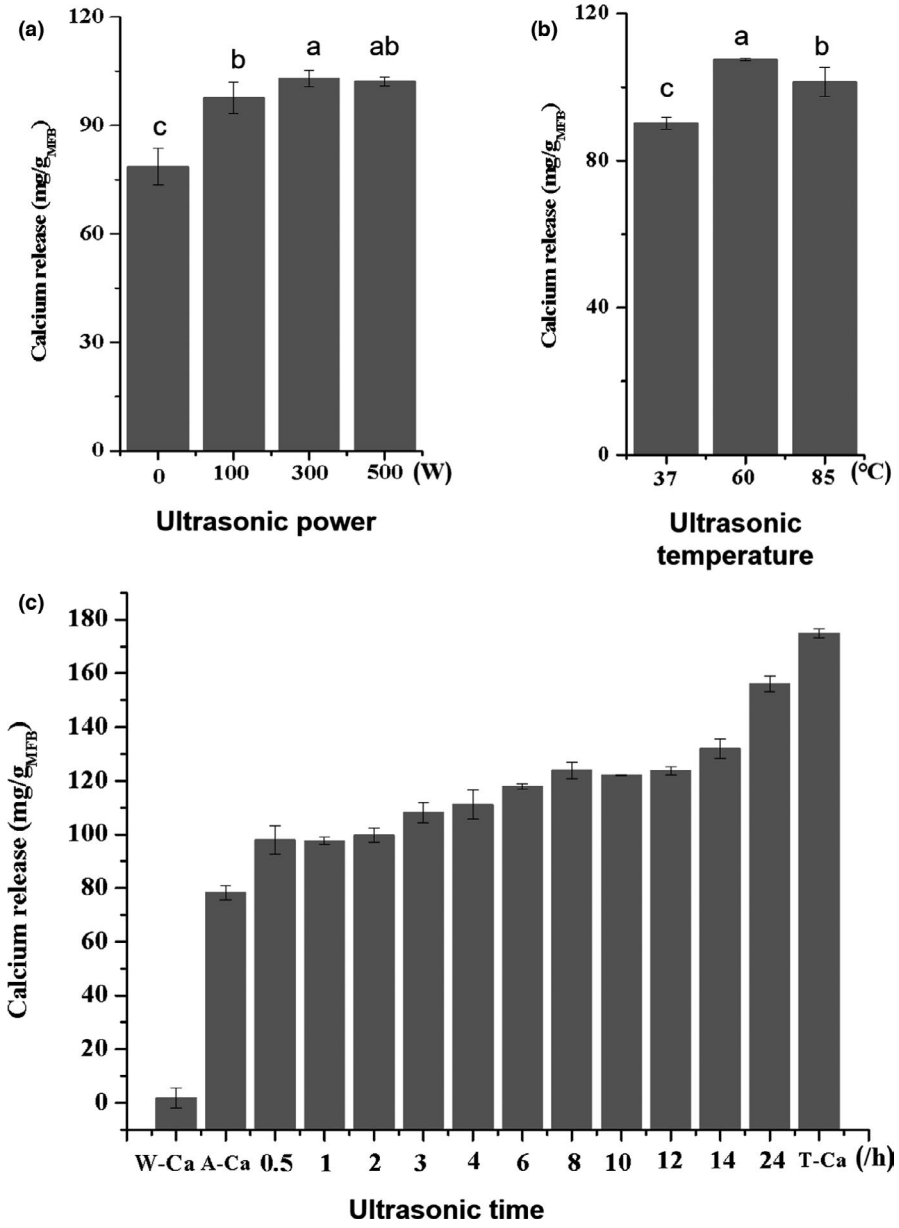

FIGURE 3 Effects of ultrasonic treatment on the calcium release mean size of MFPs. a, b, and c represent ultrasonic power, temperature, and time, respectively. W-Ca: content of calcium release with water treatment; A-Ca: content of calcium release with acid hydrolysis treatment; T-Ca: total content of calcium

TABLE 2 Equation parameters fitted to calcium release data for MFPs during ultrasonic treatment

		Fitted parameters		
Equation	Measured R_0	R_0	k	R^2
Higuchi function (Equation 1)	78.6723	82.3966	13.7125	0.9941
Zero-order kinetic function (Equation 2)		95.3910	2.6008	0.9010

FT-IR bands corresponding to hydroxyapatite and MCFs (Figure 5). After ultrasonic treatment, the amide A and B bands of collagen shifted and their intensity decreased, suggesting that collagen was gradually degraded, similar to the analysis of nanoscale fish bone particles after thermal treatment (Jiang et al., 2020). Peaks in the range from 1,646 to 1,652 cm^{-1} corresponding to the C=O stretching vibration assigned to the amide I band, characteristic of collagen, were not detected in control samples, whereas the 1,652 cm^{-1} band was observed in all U-MFP samples, except 85°C. In addition, the amide III band (1,400–1,460 cm^{-1}) is a combination of C-N stretching and N-H deformation and is also characteristic of collagen. All the samples displayed the bands at 1,460.45 and 1,411.76 cm^{-1}, but their intensity decreased after ultrasonication. The amide I bands of collagen were intense and the amide III bands were attenuated in U-MFP spectra. Both these spectral changes indicate a reduction in hydrogen bonding (Ahmed et al., 2019; Dhara, 2010). Hydrogen

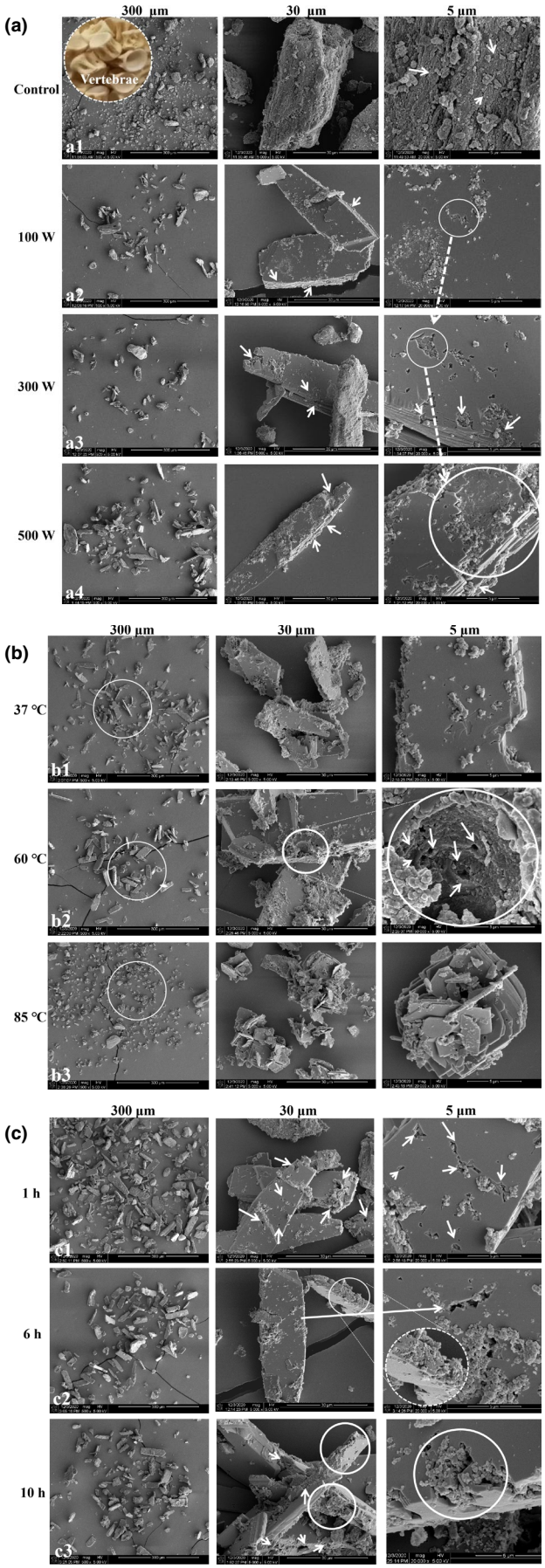

FIGURE 4 Effects of ultrasonic treatment on the surface morphology of MFPs. a, b, and c represent ultrasonic power, temperature, and time, respectively. Arrows show the structural changes in density and aperture

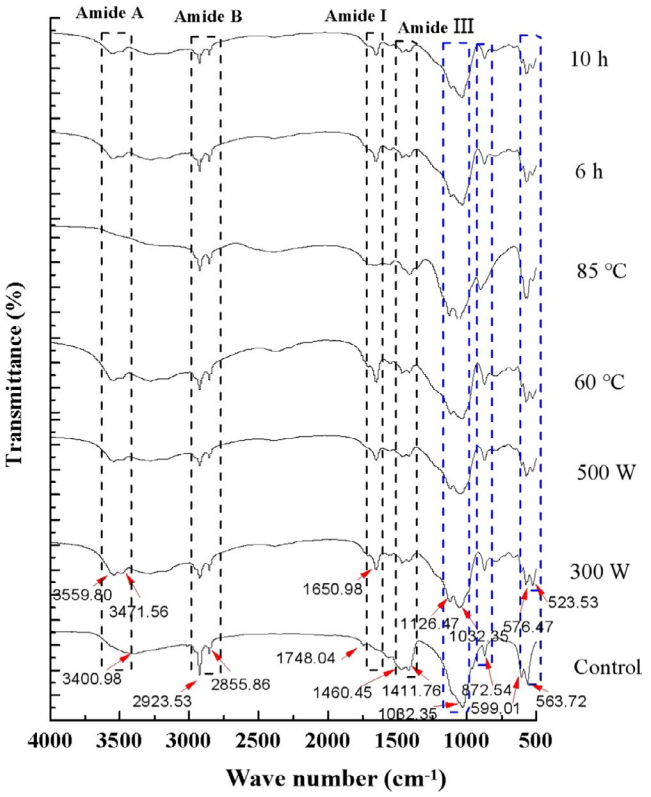

FIGURE 5 FT-IR spectra of MFPs during ultrasonic treatment

bonding is the main stabilizing interaction of the α-helical peptide chains forming the triple helical structure of collagen (Bhattacharjee & Bansal, 2010), and the weakening of these interactions in U-MFPs suggests that the collagen structure had been partially denatured.

The characteristic bands of hydroxyapatite, at 1,010–1,050 cm^{-1} (v_3 stretching mode), 960 cm^{-1} (v_1 stretching mode), 599–605 cm^{-1} (v_4 stretching mode), and 560–565 cm^{-1} (bending mode) are assigned to PO_4^{3-} groups (Liu et al., 2003). Control MFPs displayed bands at 1,032.35, 599.01, and 563.72 cm^{-1}. After ultrasonication, the band at 1,032.35 cm^{-1} shifted and split into bands at 1,126.47 and 1,032.35 cm^{-1}. The bands at 599.01 and 563.72 cm^{-1} also shifted and their separation decreased. The shifted, split, and attenuated of the PO_4^{3-} groups in U-MFPs spectra suggested that the hydroxyapatite crystal structure had also been partially disrupted (Yin et al., 2016). Hydroxyapatite is a three-dimensional network of PO_4 tetrahedra, which are linked together by columns of ninefold coordinated Ca1 atoms (Ivanova et al., 2001). The spectral changes in the PO_4^{3-} FT-IR bands after ultrasonic treatment indicate that PO_4^{3-} (or calcium) escaped from hydroxyapatite and that the crystallinity of hydroxyapatite was

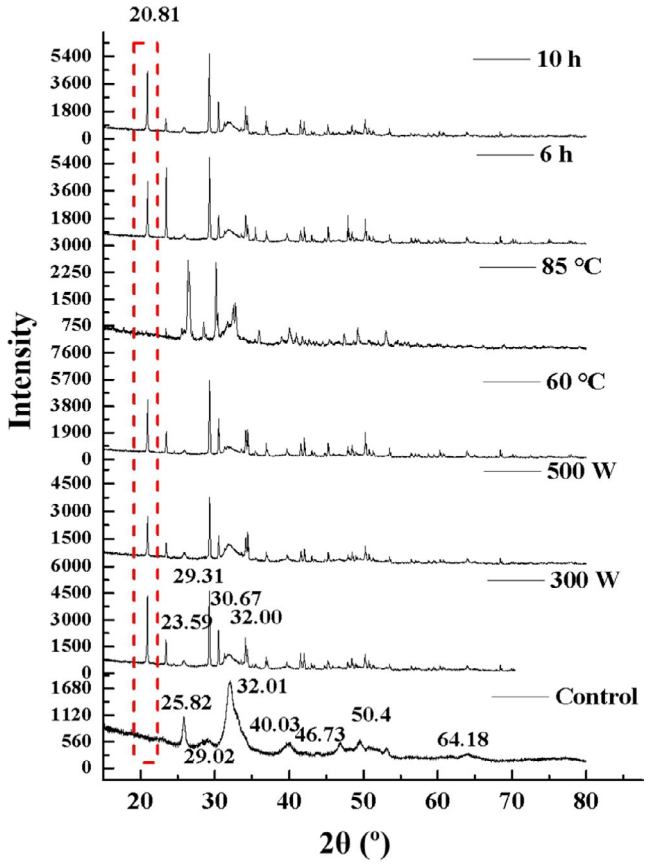

FIGURE 6 XRD spectra of MFPs during ultrasonic treatment

reduced. Partly amorphous hydroxyapatite could convert into a hydrated, highly water-soluble form, promoting the dissolution of PO_4^{3-} groups and promoting calcium release into solution (Jiang et al., 2020; Wei et al., 2011).

3.3.3 | X-ray diffraction analysis

X-ray diffraction was also used to detect the changes to the crystalline structure of hydroxyapatite and MCFs. XRD patterns of MFPs with or without ultrasonication are shown in Figure 6. Peaks at 2θ = 25.82°, 29.02°, 32.01°, 40.03°, 46.73°, 49.4°, and 64.18° are the characteristic peaks of hydroxyapatite (Das et al., 2018; Jiang et al., 2020). The untreated control samples exhibited the characteristic peaks of intact hydroxyapatite crystals, but no peaks of crystalline collagen, indicating that the crystallinity of collagen was disrupted by the presence of hydroxyapatite crystals. The MCFs in MFPs are tightly packed in parallel arrays and act like an adhesive, bonding hydroxyapatite, and thereby distorting the crystalline structure of the collagen, so it cannot be detected by XRD (Zhang et al., 2017). After ultrasound treatment, the characteristic peak of crystalline collagen at 21° (Nogueira et al., 2019) appeared and those of hydroxyapatite at 32.01° and 25.82° both shifted and weakened. The peak intensity and sharpness of the peak at 25.82° decreased and a new peak at 23.41° appeared. The broad peak at 32.01° greatly decreased in intensity and two sharp and intense peaks appeared at 29.28° and 30.61°. These spectral changes indicated that the crystal structure of hydroxyapatite was disrupted and some of the hydroxyapatite was released from the MFPs; thereafter, the collagen appeared to rearrange into its preferred crystalline structure. These findings are different from those for nanomilling, which also attenuated the characteristic peaks of collagen (Jiang et al., 2020).

4 | CONCLUSION

Taken together, the findings of this study indicated that ultrasonic treatment promoted calcium release from micrometer-scale fish bone particles (MFPs). Ultrasonication at 300 W, 60°C and for 2 h increased calcium release by 25.6% and calcium release reached 94.0% of total calcium, after 24 h ultrasonication. Overall, these findings demonstrate that ultrasonication can disrupt the crystalline structure of hydroxyapatite, promoting its dissolution, but did not denature the crystalline triple helical structure of collagen in the MCFs, only loosened and opened it up, allowing the hydroxyapatite crystals to escape. Ultrasonication may be a practical alternative to nanomilling for industrial processing of waste fish bones to produce soluble calcium as an ingredient in calcium supplements and supplemented foods.

ACKNOWLEDGMENTS

This work was supported by the Introduce High-Level Talent Team Project of Quanzhou (No.2018CT004), National Natural Science Foundation of China (No.32001625), and the Talent Introduction and Research Launch Project of Quanzhou Normal University (No. H19007).

CONFLICT OF INTEREST

The authors declare that they do not have any conflict of interest.

ETHICAL APPROVAL

Informed Consent: Written informed consent was obtained from all study participants.

DATA AVAILABILITY STATEMENT

Data are available on request from the authors.

ORCID

Juanjuan Guo https://orcid.org/0000-0003-2670-7349

REFERENCES

Ahmed, R., Haq, M., & Chun, B. S. (2019). Characterization of marine derived collagen extracted from the by-products of bigeye tuna (*Thunnus obesus*). *International Journal of Biological Macromolecules*, *135*, 668–676. https://doi.org/10.1016/j.ijbiomac.2019.05.213

Akram, A. N., & Zhang, C. (2020). Extraction of collagen-II with pepsin and ultrasound treatment from chicken sternal

cartilage; physicochemical and functional properties. *Ultrasonics Sonochemistry*, *64*, 105053. https://doi.org/10.1016/j.ultsonch.2020.105053

Ali, A. M. M., Kishimura, H., & Benjakul, S. (2018). Extraction efficiency and characteristics of acid and pepsin soluble collagens from the skin of golden carp (*Probarbus jullieni*) as affected by ultrasonication. *Process Biochemistry*, *66*, 237–244. https://doi.org/10.1016/j.procbio.2018.01.003

Ali, A. M. M., Kishimura, H., & Benjakul, S. (2018). Physicochemical and molecular properties of gelatin from skin of golden carp (*Probarbus jullieni*) as influenced by acid pretreatment and prior-ultrasonication. *Food Hydrocolloids*, *82*(9), 164–172.

Amiri, A., Sharifian, P., & Soltanizadeh, N. (2018). Application of ultrasound treatment for improving the physicochemical, functional and rheological properties of myofibrillar proteins. *International Journal of Biological Macromolecules*, *111*, 139–147. https://doi.org/10.1016/j.ijbiomac.2017.12.167

Bastami, T. R., & Entezari, M. H. (2012). Synthesis of manganese oxide nanocrystal by ultrasonic bath: Effect of external magnetic field. *Ultrasonics Sonochemistry*, *19*(4), 830–840. https://doi.org/10.1016/j.ultsonch.2011.11.019

Bhattacharjee, A., & Bansal, M. (2010). Collagen structure: The madras triple helix and the current scenario. *IUBMB Life*, *57*(3), 161–172. https://doi.org/10.1080/15216540500090710

Brodkorb, A., Egger, L., Alminger, M., Alvito, P., Assuncao, R., Ballance, S., Bohn, T., Bourlieu-Lacanal, C., Boutrou, R., Carriere, F., Clemente, A., Corredig, M., Dupont, D., Dufour, C., Edwards, C., Golding, M., Karakaya, S., Kirkhus, B., Le Feunteun, S., … Recio, I. (2019). INFOGEST static in vitro simulation of gastrointestinal food digestion. *Nature Protocols*, *14*(4), 991–1014. https://doi.org/10.1038/s41596-018-0119-1

Chen, Y. D., Fan, S. L., Yun, W. J., Chen, T. Y., & Lu, C. Q. (2007). Applications of ultrasonication in the decalcification of pathology specimens containing bone or psammoma bodies. *Zhonghua Bing Li Xue Za Zhi Chinese Journal of Pathology*, *36*(10), 708–709.

Das, T. K., Bhawal, P., Ganguly, S., Mondal, S., Remanan, S., Ghosh, S., & Das, N. C. (2018). Synthesis of hydroxyapatite nanorods and its use as a nanoreinforcement block for ethylene methacrylate copolymer matrix. *Polymer Bulletin*, *76*, 3621–3642.

Dhara, A. S. (2010). Isolation and characterization of fish scale collagen of higher thermal stability. *Bioresource Technology*, *101*(10), 3737–3742.

Eskin, D., Zhupanska, O., Hamey, R., Moudgil, B., & Scarlett, B. (2005). Microhydrodynamic analysis of nanogrinding in stirred media mills. *AIChE Journal*, *51*(5), 1346–1358. https://doi.org/10.1002/aic.10392

Ferraro, V., Carvalho, A. P., Piccirillo, C., Santos, M. M., Castro, P. M. L., & Pintado, M. E. (2013). Extraction of high added value biological compounds from sardine, sardine-type fish and mackerel canning residues — A review. *Materials Science and Engineering: C*, *33*(6), 3111–3120. https://doi.org/10.1016/j.msec.2013.04.003

Ivanova, T. I., Frank-Kamenetskaya, O. V., Kol'tsov, A. B., & Ugolkov, V. L. (2001). Crystal structure of calcium-deficient carbonated hydroxyapatite. Thermal decomposition. *Journal of Solid State Chemistry*, *160*(2), 340–349. https://doi.org/10.1006/jssc.2000.9238

Jeong, M. S., Cho, H. S., Park, S. J., Song, K. S., Ahn, K. S., Cho, M.-H., & Kim, J. S. (2013). Physico-chemical characterization-based safety evaluation of nanocalcium. *Food and Chemical Toxicology*, *62*, 308–317. https://doi.org/10.1016/j.fct.2013.08.024

Jiang, Y., Zhang, M., Yin, T., Du, H., Xiong, S., Cao, L., & Liu, R. (2020). Small-size effect on physicochemical properties of micronized fish bone during heating. *Journal of Food Processing and Preservation*, *44*(5), 1–9. https://doi.org/10.1111/jfpp.14408

Li, J., Yin, T., Xiong, S., Huang, Q., You, J., Hu, Y., Liu, R., & Li, Y. (2020). Mechanism on releasing and solubilizing of fish bone calcium during nano-milling. *Journal of Food Process Engineering*, *43*(4), 1–9. https://doi.org/10.1111/jfpe.13354

Liew, P. E., Shanmugarajah, B., Chew, I. M. L., Choong, T. S. Y., & Tan, K. W. (2015). Ultrasound assisted extraction of nano calcium from waste eggshell: A preliminary study on crystal violet dye removal. *Chemical Engineering Transactions*, *45*(2015), 1711–1716.

Liu, L., Zhang, L., Ren, B., Wang, F., & Zhang, Q. (2003). Preparation and characterization of collagen-hydroxyapatite composite used for bone tissue engineering scaffold. *Artificial Cells, Blood Substitutes, and Immobilization Biotechnology*, *31*(4), 435–448. https://doi.org/10.1081/BIO-120025414

Marliana, A., Fitriani, E., Ramadhan, F., Suhandono, S., Yuliani, K., & Windarti, T. (2015). *Synthesis and characterization of hydroxyapatite from fish bone waste* (pp. 40006). AIP Publishing LLC.

Milan, L., & Trachtenberg, M. C. (1981). Ultrasonic decalcification of bone. *American Journal of Surgical Pathology*, *5*(6), 573–579. https://doi.org/10.1097/00000478-198109000-00006

Nam, P. V., Hoa, N. V., & Trung, T. S. (2019). Properties of hydroxyapatites prepared from different fish bones: A comparative study. *Ceramics International*, *45*(16), 20141–20147. https://doi.org/10.1016/j.ceramint.2019.06.280

Neppolian, B., Wang, Q., Jung, H., & Choi, H. (2008). Ultrasonic-assisted sol-gel method of preparation of TiO2 nano-particles: Characterization, properties and 4-chlorophenol removal application. *Ultrasonics Sonochemistry*, *15*(4), 649–658. https://doi.org/10.1016/j.ultsonch.2007.09.014

Nogueira, S. S., Araujo-Nobre, A., Mafud, A. C., Guimarães, M., & Cardoso, V. S. (2019). Silver nanoparticle stabilized of hydrolyzed collagen/natural polymers based: Synthesis, characterization and antibacterial-antifungal evaluation. *International Journal of Biological Macromolecules*, *135*, 808–814.

Sricharoen, P., Limchoowong, N., Nuengmatcha, P., & Chanthai, S. (2020). Ultrasonic-assisted recycling of Nile tilapia fish scale biowaste into low-cost nano-hydroxyapatite: Ultrasonic-assisted adsorption for Hg(2+) removal from aqueous solution followed by "turn-off" fluorescent sensor based on Hg(2+)-graphene quantum dots. *Ultrasonics Sonochemistry*, *63*, 104966. https://doi.org/10.1016/j.ultsonch.2020.104966

Terzioglu, P., Ogut, H., & Kalemtas, A. (2018). Natural calcium phosphates from fish bones and their potential biomedical applications. *Materials Science & Engineering. C, Materials for Biological Applications*, *91*, 899–911. https://doi.org/10.1016/j.msec.2018.06.010

Wei, W., Zhang, X., Cui, J., & Wei, Z. (2011). Interaction between low molecular weight organic acids and hydroxyapatite with different degrees of crystallinity. *Colloids & Surfaces A Physicochemical & Engineering Aspects*, *392*(1), 67–75. https://doi.org/10.1016/j.colsurfa.2011.09.034

Xu, Y., Ye, J., Zhou, D., & Su, L. (2020). Research progress on applications of calcium derived from marine organisms. *Scientific Reports*, *10*(1), 18425. https://doi.org/10.1038/s41598-020-75575-8

Yin, T., Du, H., Zhang, J., & Xiong, S. (2016). Preparation and characterization of ultrafine fish bone powder. *Journal of Aquatic Food Product Technology*, *25*(7), 1045–1055. https://doi.org/10.1080/10498850.2015.1010128

Yin, T., Park, J. W., & Xiong, S. (2015). Physicochemical properties of nano fish bone prepared by wet media milling. *LWT - Food Science and Technology*, *64*(1), 367–373. https://doi.org/10.1016/j.lwt.2015.06.007

Zhang, J., He, S., Kong, F., Huang, S., Xiong, S., Yin, T., Du, H., Liu, R., & Zhang, M. (2017). Size reduction and calcium release of fish bone particles during nanomilling as affected by bone structure. *Food and Bioprocess Technology*, *10*(12), 2176–2187. https://doi.org/10.1007/s11947-017-1987-z

Zhang, J., Yin, T., Xiong, S., Li, Y., Ikram, U., & Liu, R. (2016). Thermal treatments affect breakage kinetics and calcium release of fish bone particles during high-energy wet ball milling. *Journal of Food Engineering*, *183*, 74–80. https://doi.org/10.1016/j.jfoodeng.2016.03.027

How to cite this article: Guo, J., Zhu, S., Chen, H., Zheng, Z., & Pang, J. (2022). Ultrasound-assisted solubilization of calcium from micrometer-scale ground fish bone particles. *Food Science & Nutrition*, 10, 712–722. https://doi.org/10.1002/fsn3.2696